Analysis of the Efficiency of Photothermal and Photodynamic Cancer Therapy via Nanogolds and Photosensitizers

Jui-Teng Lin*

New Vision Inc. 5F, No. 27, Lane 10, Datong Dist. Jiuquan St, Taipei, Taiwan

Abstract: Factors influencing the cancer therapy efficiency in both photothermal therapy (PTT) and photodynamic therapy (PDT) using nanogold particles and photosensitizers, respectively, are analyzed. In PTT, heat diffusion kinetics is used to calculate the temperature increase resulted from the nanogold absorption of light energy, whereas photochemical kinetics is used to find the efficacy of PDT, or the generation rate of reactive oxygen species. The critical factors of the PTT/PDT synergistic efficacy include: the concentration of the initiator (nanogold or photosensitizers) in the treated medium, the wavelength and energy of the light applied to the medium. Optimal parameters are calculated for maximum PDT efficacy. In PTT, diode laser (at 810 nm) is used to heat nanogolds (rod-shape or core-shell). In PDT, photosensitizers of riboflavin, 5-ALA, methylene blue and indocyanine green may be used with the associate light at wavelength of (365, 430 nm), (530-670 nm) and (780-850 nm) respectively. Both single light or dual light in infrared or visible wavelength are proposed to activate the photosensitizers or nanogolds. Optimization is required for maximum synergistic efficacy.

Keywords: Lasers, optimal, modeling, heat diffusion, photochemical kinetics.

1. INTRODUCTION

The use of nano-medicine has been used in bio-imaging and bio-sensing, drug delivery, cancer cell diagnostics and therapeutics [1-7]. Nano-particles can cause tumor cell death by photothermal ablation, mechanical damage, and increase in the localized drug concentration. Gold nanoparticles are promising agents for cancer therapy, drug carriers, photo-thermal agents and contrast agents. The U.S. Food and Drug Administration (FDA) has approved numerous Investigational New Drug (IND) applications for nano-formulations, enabling clinical trials for breast, gynecological, solid tumor, lung, mesenchymal tissue, lymphoma, central nervous system and genito-urinary cancer treatments.

Various nanoparticles have been explored for the use of surface plasmon resonance (SPR) including shapes in spheres, rods, boxes, cages and shells [3-6]. By changing the shape of nanoparticles from spheres to nanorods, the absorption and scattering peaks change from visible to the near-infrared (NIR) regime. Comparing to the visible light, light in the NIR regime offers the advantages of larger absorption and scattering cross sections and much deeper penetration depth in tissues [3, 8-10]. The red-shift of the absorption peak in nanorods is governed by the aspect ratio (defined by as the ratio of the length to the cross-sectional diameter), whereas it is governed by the shell thickness in nanoshells [9]. Recent studies have shown that gold nanorods conjugated to antibodies [3,5] could be used for selective and efficient photothermal therapy. Lin et a [8,11] proposed the use of a diode laser system having multiple wavelengths for more efficient treatment of cancer tumor.

Although NIR lasers for cancer therapy offers much deeper tissue penetration depth than that of visible lasers, they are limited to the normal tissues. In cancer tissues having GNRs components, its absorptions at the resonant wavelength increase significantly to about 1.5 to 5.0 cm^{-1}, depending on the GNRs concentrations. Therefore, the penetration depth in cancer tissue or tumor is still limited to about 0.1 to 0.3 cm. Overheating on the surface area of targeted tissues is always an issue to be overcome. In addition, the distribution of the GNRs aspect ratios and their concentrations inside the cancer tissues or tumors are also difficult to be controlled for perfectly matching the laser peak absorption. To overcome the penetration issue, Lin et al proposed the use of a train-pulse to increase the volume temperature increase [11] which is particularly useful to larger volume tumors, unless an inserting fiber is used to deliver the laser energy.

New synergistic treatment modalities combining PDT with PTT could overcome current limitations of PDT, thus achieving enhanced anticancer efficacy. To promote the tumor accumulation of PS and to generate heat for synergistic PDT/PTT, surface conjugation of PS on nanoparticles has been proposed, which however, has limitations including relatively low loading capacity and the possible leakage of PSs coupled on NP surfaces during their circulation in biological systems [12].

*Address correspondence to this author at the New Vision Inc. 5F, No. 27, Lane 10, Datong Dist. Jiuquan St, Taipei, Taiwan; Tel: 886+961306877; Fax: 886-25932028; E-mail: jtlin55@gmail.com

ISSN: 1929-2260 / E-ISSN: 1929-2279/17

In this study, we will present the factors influencing the cancer therapy efficiency in both photothermal therapy (PTT) and photodynamic therapy (PDT) using nanogold particles and photosensitizers, respectively. In PTT, heat diffusion kinetics is used to calculate the temperature increase resulted from the nanogold absorption of light energy, whereas photochemical kinetics is used to find the efficacy of PDT, or the generation rate of reactive oxygen species. The critical factors of the synergistic therapy efficiency to be discussed include: the concentration of the initiator (nanogold or photosensitizers) in the treated medium, the wavelength, energy and the irradiation period of the light applied to the medium. Optimal parameters are calculated for maximum PDT efficacy.

2. METHODS AND DISCUSSIONS

2.1. The Modeling System

As shown in Figure **1**, the tumor cells killing efficiency may be enhanced by combining the photothermal therapy (PTT) and photodynamic therapy (PDT) using two light sources (either lasers or LED sources), in which the treated tumor tissue is injected by both nanogold solution and photosensitizers. Depending on the types of photosensitizers and the shapes of the nanogold, the light wavelengths matching the absorption may vary from UV, visible to near IR (NIR). For examples, nanosphere absorbs visible light (at 480-680 nm), nanocube (700-900 nm), nanorod (700-2500 nm), and nanoshell (480-810 nm).

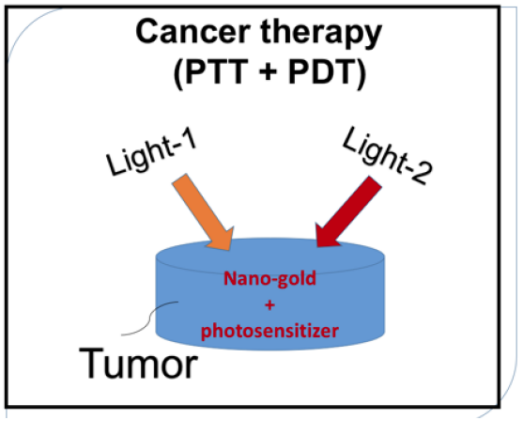

Figure 1: Schematics of a combined PTT and PDT processes using 2 lights acting on the tumor injected with nanogold solution and photosensitizer.

As shown in Figure **2**, the combined PTT and PDT processes using various lights having wavelength from UV to IR with associate nanogold shapes and photosensitizer. Photosensitizer riboflavin (B2), 5-ALA, methylene blue (MB) and indocyanine green absorb, respectively, light at wavelength of (365, 430 nm), (530-670 nm), (780-850 nm), as shown by Figure **2** [13-16]. Therefore, a combined dual-function of PTT/PDT can be performed by: (i) an NIR light at NIR absorbed by gold nanorod and indocyanine green; or a visible light absorbed by gold nanosphere and 5-ALA; (b) two different lights having wavelength at NIR (for PTT) and UV to visible light (for PDT). For the case of one light for both PTT and PDT the simultaneously interacting with the nanogold and the photosensitizer is much more complex than that of the case of two different lights which can be treated independently. We will start with the simple case, where PTT and PDT will be modelled by the heat diffusion equation and the kinetic equation, respectively, as follows.

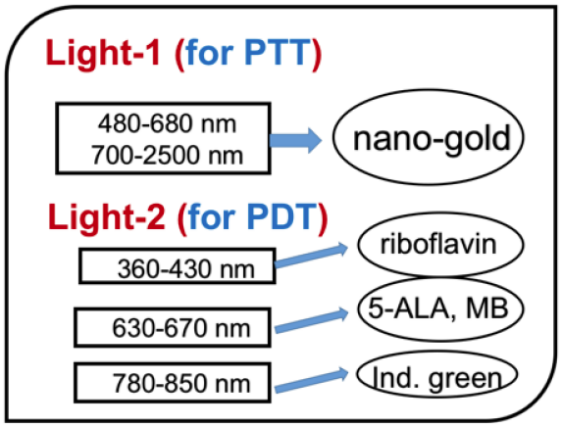

Figure 2: Combined PTT and PDT processes using various lights having wavelength from UV to IR with associate nanogold shapes and photosensitizer.

2.2. The Temperature Increase in PTT

As shown in Figure **3**, an experimental setup for a diode laser system with fiber coupled three wavelengths at 808, 852 and 915 nm [11]. The surface and volume temperature increases of the GNR solution were measured. Figure **4** shows the cell viability at irradiation time of 90 and 120 seconds at laser power 1.0 W using a diode laser at 808 nm [7].

The temperature profile of the laser irradiated GNR solutions of the above described experimental setup may be solved numerically by a heat diffusion equation as follows [11,17]

$$\frac{\partial^2 T}{\partial z^2} - \frac{1}{k}\frac{\partial T}{\partial t} = -G(z) \tag{1.a}$$

$$G(z) = \left(\frac{AI}{K}\right) e^{-BZ} \tag{1.b}$$

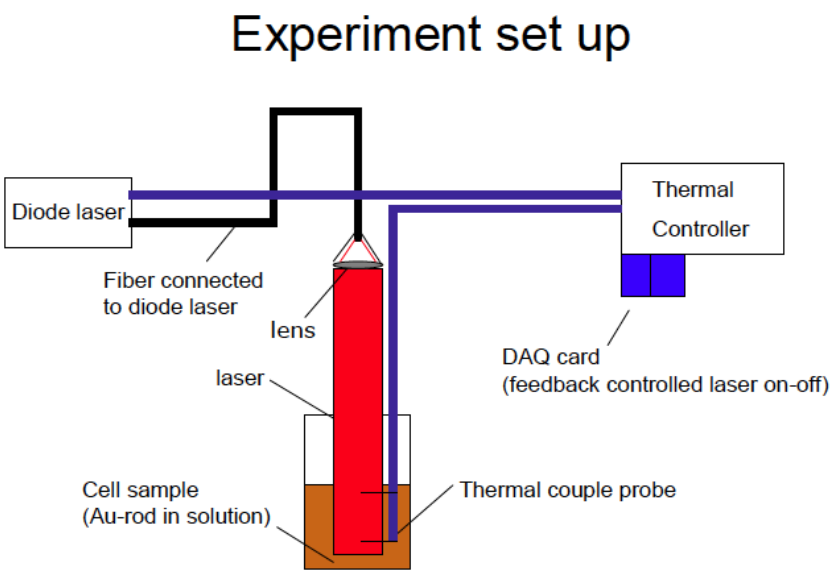

Figure 3: Experimental setup for a diode laser system with fiber-coupled three wavelengths (808 nm, 852 nm and 915 nm), bundled to one single external fiber connected to a hand piece and a collimation lens. Two thermal couples were inserted into the GNR solution at z=1.5 and 5.0 mm to measure the surface and volume temperature of the GNR solution [11].

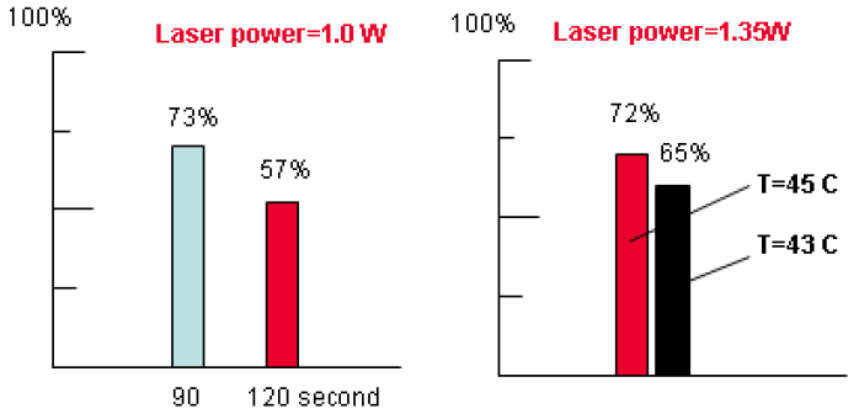

Figure 4: The cell viability at irradiation time of 90 and 120 seconds at laser power 1.0 W (left figure); right figure shows cell viability at a given irradiation time of 60 seconds and laser power of 1.35 W, for different preset surface temperatures (T=43 and 45^0C). The higher surface temperature kills more cancer cells as expected [7].

where z is the laser propagation direction along the depth of the GNRs solution, k and K are, respectively, the thermal conductivity and diffusivity of the solution, I is the laser intensity (or power density), B is the extinction coefficient, which can be expressed by $B=[A(A+2s)]^{1/2}$, where A and s are the absorption and scattering coefficient. In this study we will assume that the scattering is much smaller than the absorption, and B=A. We note that A is proportional to the product of the extinction coefficient and concentration of the GNRs.

The above heat diffusion equation is solved numerically under the initial and boundary conditions: $T(z,0) = T_0$, dT/dz (at $z=0$) $= h\,[T(0, z)-T_0]/k$, where h is the heat transport coefficient due to the air convection of the GNRs solution surface. Typical thermal parameters to be used in our calculations are K=0.0045 (WC/cm), k=0.00149 (cm^2/s), and h=0.01 (WC/cm^2) [16]. We shall use above theory to study and compare with the measured data showing the roles of A and F on the temperature profiles near the surface and inside the GNRs solutions. When the irradiation time is much longer than the thermal relaxation time, the laser-heated solution will reach a steady-state which is analytically available [17].

The light source terms G(z) have an optimal value. By taking dS/dA (A=A*)=0, one obtains the maximal G*=I/(zK) under the optimal condition A*=1/z. The maximal G* is resulted from the competing function of A and exp(-Az). The optimal A* also indicates that

there is an optimal concentration of GNRs. We will show later that this optimal feature also exists for the photosensitizer concentration in the photodynamic process.

We first study the role of laser intensity (I) on the surface-temperature increase. We measured the laser illumination time needed (defined as t2, in seconds) for the near-surface (z=1.5 mm) temperature increase of 10^0C, that is from an initial temperature of 25^0C to 35^0C. Using an 808-nm diode laser (having a measured A=3.5 cm^{-1}) for various laser intensity I=0.5 to 4.0 (W/ cm^2). The measured t2 values are decreasing function of the laser intensity (I). We also calculated laser illumination time needed for various A values indicating that larger (AI) values have a shorter time needed to reach a specific temperature increase.

In the pulsed train technique, custom-designed Labview software was used for feedback controlling the laser on/off times such that a preset surface-temperature is achieved. We analyze the roles of A and I on the temperature increase profiles (dT).

For case (a): fixed A and change I. The measured surface- and volume-temperature increase profiles (dT) of the experiment described earlier, at positions z=1.5 and 5.0 mm, respectively, for a diluted GNRs solution (with A=1.33 cm^{-1}) heated by various laser intensity of I=(1.0, 2.0, 2.9) W/cm^2. In these measurements, we controlled the surface-dT to be about 10^0C (with a bandwidth about 0.25^0C) by the pulsed train on-off technique such that the volume-dT (at z=5.0 mm) reaches about 8^0C, which can not be achieved in cw mode operation without overheating the solution surface. In addition, larger I shows faster surface-dT rising profile and higher volume-dT inside the solution.

For case (b): fixed AI, change A and I. The measured temperature increase profile (dT) due to a diode laser at 808 nm (with A=2.9 cm^{-1}) and at 852 nm (with A=2.0 cm^{-1}) for a fixed AI=2.9 (W/cm^3). These data show that smaller A (with larger F) has a faster rising surface-dT profiles and higher volume temperature. These features could also be realized by observing the laser heating term of Eq. (1), (AI/K)exp(-Bz), which indicates that the temperature increase profile (dT) is proportional to the combined factor of (AI/K). However larger A-value will cause a lower dT due to the stronger exponential absorbing (decaying) term exp(-Bz). This non-linear competing behavior of A on the profiles of dT shown by the heat diffusion equation is demonstrated by our measured results.

We should note that the pulsed-train on-off method [11] along can not increase the volume-dT to the desired value. One shall also require an optimal A value (say about 1.0 cm^{-1} to 1.5 cm^{-1}) which may be controlled either by the GNRs concentration or by using specific off-resonance laser wavelengths. It should be noted that the A-value can not be too small (say <0.5 cm^{-1}) which will require a longer time needed (say >60 seconds) for a surface-dT about 10^0C.

The novel features demonstrated in the above described also imply that cancer tumor having a dimension of 10x10mm can be treated using the pulsed train method presented in this paper, but not by the conventional single pulse method. That is to say any cancer tumor with size over 5.0 mm can not be treated via conventional single pulse method, unless the surface is overheated.

In the above examples, we have clearly demonstrated both experimentally and theoretically that the volume dT could be significantly increased to treat large size tumors using the combined techniques of: (a) the pulsed train operation, and (b) the optimal control of the laser intensity and the absorption coefficients for a given GNRs aspect ratio and concentration. This study provides us a general guidance that for clinically optimized condition of 10 to 40 seconds laser irradiation time to kill the cancer tumor with size of 0.5 to 1.5 cm diameter, one should use a laser intensity about (1.0 – 3.0) (W/cm^2) and control the A values about (0.8-2.0) cm^{-1}. Furthermore, the pulsed-train (on-off) technique is required in order to avoid surface overheating.

We should note that the *in vivo* situation in animal and/or human cancer therapy will be much more complex than the *in vitro*, simplified conditions described in this paper. These complexities shall include the non-uniform GNRs concentration in the tumor, the multi-layer normal-cancer tissue medium with multiple thermal parameters, and the blood flowing of the laser-targeted areas. This study with simplified conditions defined by uniform GNRs solution and controlled thermal parameters, however, still provides meaningful guidance based on vitro experimental measurements which are also consistent with theory. In addition, the design of multiple-wavelengths laser system shall partially overcome the issues of GNRs non-uniform and multiple thermal medium for a 3-dimensional-therapy, in which various absorption penetration depths are available via the fiber-coupled

multiple-wavelength laser simultaneously targeting the cancer tumors, Finally, the novel techniques and the laser system with auto-temperature control introduced in this paper should provide useful tool for animal studies which are in progress in our lab, where a faster temperature response time (about 150 ms) given by an IR camera will be integrated to our existing system for real-time surface temperature monitoring.

2.3. The Kinetic of PDT

We shall now discuss the PDT process which utilizes reactive oxygen species (ROS) generated through the reaction between photosensitizer (PS) and oxygen presented in tissues upon the irradiation of light to achieve effective treatment. The ROS is generated under a so-called type-II photochemical reaction which requires oxygen and the PS concentration is not depleted. In comparison, PS concentration is depleted under a type-I process. We will consider the case that the same light is absorbed by both the PS and the nanogold. It reduces to the simpler situation when two light with different wavelengths are absorbed respectively by the PS and nanogold, in which the PTT and PDT can be treated independently.

Combining PTT and PDT, the kinetic equations of the light intensity I(z,t) and the PS concentration C(z,t) is given by [18,19]

$$\frac{\partial C(z,t)}{\partial t} = -a' I(z,t) C(z,t) \tag{2.a}$$

$$\frac{\partial I(z,t)}{\partial z} = -[(a-b) C(z,t) + bC_0 + A + Q] I(z,t) \tag{2.b}$$

where *a'=ap* with *p* being the quantum yield for a type-I process; Q is the tissue absorption coefficient without nanogold or PS; A is the absorption constant of the nanogold; *a* and *b* are the extinction coefficient of the PS and the photolysis product having an concentration C(z,t) with initial value C_0. It is important to note that Eq. (2.a) showing that C(z,t) is coupled to the light intensity via *a'=ap* which is only depending on the quantum yield for a type-I process, and not depending on the quantum yield for a type-II process, in which the PS concentration is not depleted. Eq. (2.b) also includes the light intensity reduction due to the absorption by nanogold via the exp(-Az) term, when the same light is used for both PTT and PDT. We note that stronger PTT (or larger Az) produces higher temperature, which however also reduces the available light intensity for PDT. Therefore, there is an optimal condition depending upon either PTT or PDT will be our dominated process for optimal clinical outcomes.

Eq. (2) requires numerical solutions due to the PS concentration depletion in type-I process. Approximate analytic solutions are given by [19]

$$I(z,t) = I_0 \exp[-(a-b) z C(z,t) - bzC_0 - (A+Q)z] \tag{3.a}$$

$$C(z,t) = C_0 \exp(-a'E) \tag{3.b}$$

where *E'* is numerically fit as $E=(E_0-g)\ exp(-A'z)$ which is propositional to the initial light energy $E_0=tI_0$ and $A'=bC_0+A+Q$. Therefore, smaller A, or lower PTT temperature increase, C(z,t) is higher for larger PDT effects. This competing process between PTT and PDT requires an optimization for maximum therapy efficacy.

In general, both type-I and type-II reactions occur in the photochemical reaction. The kinetic equation of the the photoinitiation rate for type-I (R_1) process and type-II (R_2) generation of the reactive oxygen species (ROS) is given by [19]

$$\begin{aligned} \frac{d[M]}{dt} &= R_1(z,t) + R_2(z,t) \\ &= K_0 \left[\sqrt{a'p} + \sqrt{q}\right] \sqrt{C(z) I(z)} \end{aligned} \tag{4}$$

where *p* and *q* are the quantum yield for type-I and type-II process, respectively. In general, the quantum yield for a type-II process (*q*) is time-dependent due to the depletion of the required-oxygen in the generation of ROS.

Type-I process defines the efficacy for polymerization (or crosslinking) and type-II process defines the efficacy of PDT, or the total amount of ROS generated. Integration of Eq. (4) over z, and taking average over the depth (z), we obtain the normalized [M] per unit depth [19]

$$\begin{aligned} \frac{S(z,t)}{K_0} &= \frac{1}{zK_0} \int_0^z R_2(z',t') dt' dz' \\ &= \frac{1}{zK_0} \int_0^z [M(z)] dz' \end{aligned} \tag{5}$$

which can be solved only numerically and analytic equation was shown earlier for the case for PDT only, or when PTT is neglected, or the Az term in Eq. (3) is neglected [19].

Eq. (5) shows that [M(z)] has an optimal azC_0 or optimal depth (z*) and concentration, with z* is

proportional to ln(E)/(A'+A). It also shows an optimal light energy (E), however, longer exposure time (or higher intensity) has higher S for a given energy. Figure **5** shows the typical profiles of [M(z)], for various light energy of 1.0 to 7.0 J/cm^2 (for curves 1 to 7). We note that [M(z)] has optimal depth which is an increasing function of the light energy.

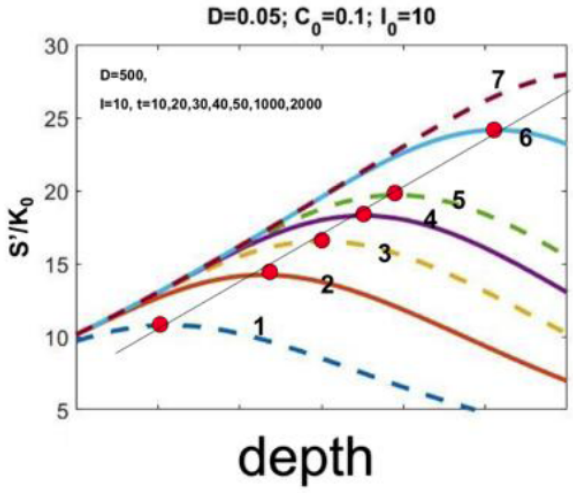

Figure 5: Profiles of [M(z)] in type-I process for various light energy of 1.0 to 7.0 J/cm^2 (for curves 1 to 7) [19].

2.4. The Combined PTT/PDT Efficacy

Eq. (3) and (4) show the following important features for the PDT efficacy defined by the amount of ROS generation. [M] is an increasing function of the light energy (or intensity x time) and its quantum yield (*q*). However, it is reduced by the PS concentration depletion occurring in type-I process (with a quantum yield *p*). For maximum PDT efficacy one requires the following conditions: small *p* (or weak type-I process), large *q* (or sufficient oxygen supply during the reaction), small *A* (or small absorption by the nanogold). On the other hand, for high PTT efficacy one requires large temperature increase (dT) which is proportional to the light absorption in the nanogold, or $A'I_0$. Therefore, in case-1 using one light to perform both PTT and PDT would require higher light energy (or intensity) comparing to case-2 using two different lights for PTT and PDT, independently without co-absorption, and therefore PTT and PDT can be treated separately. In case-1 using one light for both PTT and PDT processes, the system design is simpler and cost effective. However, the collective effects between PTT and PDT requires complex optimization of the concentration of PS and nanogold, besides that the wavelength of the light must match both the absorption peak of PS and nanogold. Greater details requiring numerical solutions of Eq. (3) and (5) will be presented elsewhere.

In addition to the methods presented in this paper, the efficacy of PDT may be further improved significantly via conjugated nanogolds. For example, it was reported by the conjugated spherical nanogold as the delivery agent for 5-ALA resulted in a two times higher cell death rate compared to free 5-ALA [14]. Another example is that the DNA damage caused by PDT as demonstrated by alkaline gel electrophoresis was greater in the methylene blue (MB) plus chitosan-treated group than in control and MB-treated groups [16].

3. CONCLUSION

Efficacy of cancer therapy may be enhanced by combining PTT and PDT either activated by one light or two lights. For maximum PTT/PDT synergistic efficacy, the concentration of PS and nanogold required optimization in addition to the wavelength of the light matching the absorption peak of PS and nanogold.

CONFLICT OF INTEREST

The author is the CEO of New Vision Inc. and has financial interest.

ACKNOWLEDGEMENTS

This work was supported by the internal grant of New Vision Inc, and also partially supported by a grant from Talent-Xiamen (XM-200) program (Xiamen Science & Technology Bureau, China).

REFERENCES

[1] Tong L, Wei G, Cheng JX. Gold nanorods as contrast agents for biological imaging: optical properties, surface conjugation and photothermal effects. Photochem and Photobiol 2009; 85: 21-32. https://doi.org/10.1111/j.1751-1097.2008.00507.x

[2] West JL, Halas JN. Engineered nanomaterials for biophotonics applications: improving sensing, imaging, and therapeutics. Annu Rev Biomed Eng 2003; 5: 285-292. https://doi.org/10.1146/annurev.bioeng.5.011303.120723

[3] Huang X, El-Sayed MA. Gold nanoparticles: Optical properties and implementations in cancer diagnosis and photothermal therapy. J Advanced Research 2010; 1: 13-28. https://doi.org/10.1016/j.jare.2010.02.002

[4] Popp MK, Oubou I, Shepherd C, *et al*. Photothermal therapy using gold nanorods and near-infrared light in a murine melanoma model increases survival and decreases tumor. J Nanomaterials 2014; ID 450670.

[5] Lin J, Wang S, Huang P, *et al*. Photosensitizer-loaded gold vesicles with strong plasmonic coupling effect for imaging-guided photothermal/photodynamic therapy. ACS Nano 2013; 7: 5320-5329. https://doi.org/10.1021/nn4011686

[6] Wang YH, Chen SP, Liao AH, *et al*. Synergic delivery of gold nanorods using multifunctional microsbubbles for enhanced plasmonic photothermal therapy. Scientific Report 2014; 5685.

[7] Lin JT, Chiang S, Lin GH, *et al*. *In vitro* photothermal destruction of cancer cells using gold nanorods and pulsed-train near-infrared lase. J Nanomaterials 2012; article ID 861385. https://doi.org/10.1117/1.3543815

[8] Lin JT. Nonlinear optical theory and figure of merit of surface plasmon resonance of gold nanorods. J Nanophotonics 2011; 5: 051506. https://doi.org/10.1117/1.3525598

[9] Lin JT. Scaling law and figure of merit of biosensor using gold nanoshells. J Nanophotonics 2010; 4: 049507.

[10] Lin JT. A generalized geometric factor for unified scaling law for bio-sensor based on nanostructures of gold. Inter J Latest Res Science and Tech 2013; 2: 23-25.

[11] Lin JT, Hong YL, Chang C. Selective cancer therapy via IR-laser-excited gold nanorods. Proc SPIE 2010; 7562: 75620R-1.

[12] Wang YH, Chen SP, Liao AH, *et al.* Synergistic delivery of gold nanorods using multifunctional microbubbles for enhanced plasmonic photothermal therapy. Science Reports 2014; 4: 5685. https://doi.org/10.1038/srep05685

[13] Shemesh CS, Hardy WC, Yu DS, *et al*. Indocyanine green loaded liposome nanocarriers for photodynamic therapy using human triple negative breast cancer cells. Photodiag Photodany Therapy 2014; 2: 193-203. https://doi.org/10.1016/j.pdpdt.2014.02.001

[14] Mohammadi Z, Sazgarnia A, Rajabi O, *et al*. An *in vitro* study on the photosensitivity of 5-aminolevulinic acid conjugated gold nanoparticles. Photodiag Photodany Therapy 2013; 10: 382-388. https://doi.org/10.1016/j.pdpdt.2013.03.010

[15] Akens MK, Wise-Milestone L, Won E, *et al*. *In vitro* and *in vivo* effects of photodynamic therapy on metastatic breast cancer cells pre-treated with zoledronic acid. Photodiag Photodany Therapy 2014; 11: 422-433. https://doi.org/10.1016/j.pdpdt.2014.04.002

[16] Choi SS, Lee HK, Chae HS. Synergistic *in vitro* photodynamic antimicrobial activity of methylene blue and chitosan against Helicobacter pylori 26695. Photodiag Photodany Therapy 2014; 11: 526-532. https://doi.org/10.1016/j.pdpdt.2014.08.005

[17] Carslaw HS, Jaeger JC. Conduction of Heat in Solids; Oxford University Press: New York, 2nd Ed. 1959.

[18] Lin JT, Cheng DC. Optimal focusing and scaling law for uniform photo-polymerization in a thick medium using a focused UV laser. Polymers 2014; 6: 552-564. https://doi.org/10.3390/polym6020552

[19] Lin JT. Combined analysis of safety and optimal efficacy in UV-light-activated corneal collagen crosslinking. Ophthalmology Research 2016; 6: 1-14. https://doi.org/10.9734/or/2016/28712

Received on 26-09-2016 Accepted on 08-12-2016 Published on 16-02-2017

DOI: https://doi.org/10.6000/1929-2279.2017.06.01.2